Synchronizing a single-electron shuttle to an external drive

2014 New J. Phys. 16 043009

(http://iopscience.iop.org/1367-2630/16/4/043009)

New Journal of Physics
The open access journal at the forefront of physics
Deutsche Physikalische Gesellschaft DPG | IOP Institute of Physics

Synchronizing a single-electron shuttle to an external drive

Michael J Moeckel[1,2,3], Darren R Southworth[4], Eva M Weig[4,5] and Florian Marquardt[6]

[1] Max-Planck-Institut für Quantenoptik, Hans-Kopfermann-Str. 1, Garching D-85748, Germany
[2] Center for Computational Chemistry and Department of Chemistry, University of Cambridge, Lensfield Road, Cambridge CB2 1EW, UK
[3] St John's College Cambridge, Cambridge CB2 1TP, UK
[4] Center for NanoScience (CeNS) and Fakultät für Physik, Ludwig-Maximilians-Universität, Geschwister-Scholl-Platz 1, München D-80539, Germany
[5] Department of Physics, Universität Konstanz, Universitätsstraße 10, Konstanz D-78457, Germany
[6] Institute for Theoretical Physics, Universität Erlangen-Nürnberg, Staudtstr. 7, Erlangen D-91058, Germany
E-mail: Michael.Moeckel@gmx.de

Received 26 November 2013, revised 24 February 2014
Accepted for publication 3 March 2014
Published 11 April 2014

New Journal of Physics **16** (2014) 043009

doi:10.1088/1367-2630/16/4/043009

Abstract

The nanomechanical single-electron shuttle is a resonant system in which a suspended metallic island oscillates between and impacts at two electrodes. This setup holds promise for one-by-one electron transport and the establishment of an absolute current standard. While the charge transported per oscillation by the nanoscale island will be quantized in the Coulomb blockade regime, the frequency of such a shuttle depends sensitively on many parameters, leading to drift and noise. Instead of considering the nonlinearities introduced by the impact events as a nuisance, here we propose to exploit the resulting nonlinear dynamics to realize a highly precise oscillation frequency via synchronization of the shuttle self-oscillations to an external signal. We link the established phenomenological description of synchronization based on the ADLER equation to the microscopic nonlinear dynamics of the electron shuttle by calculating the effective ADLER constant analytically in terms of the microscopic parameters.

Keywords: nanomechanical resonators, synchronization, single electron shuttle, nonlinear dynamics, nanometrology

1. Introduction

Micro- and nanoscale resonators [1, 2] currently receive much attention both in applied and basic research. Their extreme sensitivity and design flexibility have enabled, for instance, mass sensing on the single ad-atom level [3–5], force sensitivity below the attonewton range [6–8], and access to the ultimate quantum mechanical limits of motion [9–11]. The nonlinear dynamical behavior in nanomechanical oscillators has received new attention recently, including studies of nonlinear damping [12], the use of buckling modes for mechanical information storage [13], noise reduction due to nonlinearities [14], the choice of optimal operation points [15], and signal amplification at bifurcation points [16].

One particularly important example of a nanomechanical system that can become highly nonlinear is the electron shuttle. Its nonlinear response has been demonstrated, most recently in a system of two coupled electron shuttles [17]. Nanomechanical electron shuttles [18] have the potential to administer current with single-electron accuracy. This ultimate limit of current control would allow to redefine the current standard in terms of fundamental constants [19–22], and to close the so-called 'metrological triangle' by relating voltage and resistance defined in terms of fundamental constants.

A nanomechanical electron shuttle [23–30] consists of a nanomechanical resonator carrying a metallic island which oscillates between two metallic electrodes (figure 1). The island defines a quantum dot which, if operated in the Coulomb blockade regime [31, 32], can be consistently charged with a known number of charge carriers down to the single electron level. The advantage of nanomechanical shuttles over other approaches is their inherent suppression of unwanted co-tunneling due to tunnel contact with only one electrode at a time. Given a sufficiently large dc voltage, the shuttle enters into Coulomb attraction-driven self-oscillation, where Coulombic forces drive the charged island to impact with and re-charge on subsequent electrodes [26, 27, 30], realizing a nanoscale version of Benjamin Franklin's 'lightning bell' [33].

Synchronization dynamics in nanomechanical systems has only recently been discussed both for synchronization to an external drive [34] as well as for synchronization between two nanomechanical oscillators [34–38]. In this paper, we show that synchronization to an external drive can be exploited to provide a stable and reproducible frequency for an oscillating single-electron shuttle. In combination with charge quantization [28, 29], this will ensure the desired reproducibility and precision of the shuttle current for metrological applications. We establish the requirements for this synchronization regime by analyzing the nonlinear impact dynamics of the shuttle, i.e. a dynamical regime that has received comparatively little attention so far. In doing so, we go beyond the dynamical effects of the alternating recharging of the shuttle at the electrodes [39]. Our results can be cast in the form of an effective equation (of the Adler type), where we discuss the strength of the frequency locking as a function of microscopic parameters. This will serve as a guideline for experiments that attempt to exploit the effect predicted here.

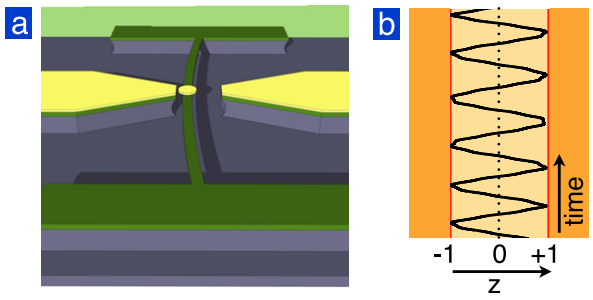

Figure 1. (a) A nanomechanical electron shuttle oscillating between and impacting on two electrodes and (b) a typical trajectory.

2. Model

We model the shuttle as a nanomechanical harmonic oscillator with eigenfrequency ω_0, effective mass m, and quality factor $Q = \omega_0/\Gamma$ using nondimensional coordinates ($z = x/L$) and time ($\tau = \omega_0 t$). Two electrodes are located at positions $x = \pm L$ and restrain its oscillatory motion such that inelastic *impact events* occur: then the velocity reverses sign and is rescaled by an impact damping parameter $\sqrt{\eta} \leqslant 1$ as kinetic energy is lost. Simultaneously, the shuttle is charged to a value $q = \pm cv$,[7] and is accelerated towards the other electrode by a force $F = qV/2L \propto V^2$. The dimensionless electrostatic force term is $\mathcal{V}^2 = \left(V/V_*\right)^2$ with $CV_*^2/2 = m\omega_0^2 L^2$; it is half the ratio between the charging energy and the oscillator's potential energy at the impact point and carries a sign depending on which electrode has been contacted last ('+' for $z = -1$). Crucial for our discussion is an additional external driving, e.g. by a periodic force $\mathcal{F}$. The equation of motion between the electrodes reads

$$\ddot{z}(\tau) + Q^{-1}\dot{z}(\tau) + z(\tau) = \mathcal{F}\cos\left(\Omega\tau\right) \pm \mathcal{V}^2 . \tag{1}$$

Our model is described by five dimensionless parameters: (i) the mechanical quality factor Q, (ii) the dimensionless amplitude $\mathcal{F}$ of the external driving force, (iii) its external driving frequency Ω, written in units of the oscillator resonance frequency ω_0, (iv) the impact damping parameter η and (v) the dimensionless voltage $\mathcal{V} \equiv V/V_*$. Figure 1 displays a typical trajectory with impact at the electrodes, under simultaneous driving.

We note that any extra intrinsic nonlinearities, while possibly present, do not alter the essential results below, since the main nonlinearity is provided by the impacts at the electrodes. The synchronization we analyze is a robust phenomenon, insensitive in its main aspects to many details of the model.

All the physical quantities of interest may be expressed by the dimensionless parameters and a few dimensional quantities. For example, the average shuttle current can be obtained from the transported charge CV and the frequency: $I = CV\omega_0\bar{\tau}^{-1}$. Here $\bar{\tau}^{-1}$ is defined as the averaged inverse (dimensionless) time for a one-way trip between the electrodes.

[7] Here we assume the charge q to be linear in the voltage V. At low temperatures, in the Coulomb blockade regime, the charge shows discrete plateaus as a function of V. Then $\mathcal{V}^2$ in equation (1) and in all of the subsequent formulas and figures must simply be replaced by $QV/\left(2m\omega_0 L^2\right)$.

2.1. Self-oscillations without external driving

When a sufficiently large dc voltage is applied to the electrodes, the acceleration by the electric field overcomes frictional losses due to impact and the shuttle can execute self-oscillations even in the absence of external resonant driving [18]. The properties of this well-known regime are crucial to our analysis as they form the reference state for a subsequent perturbative approach. In this regime, the shuttle shows regular motion, where the velocity before impact is always the same. We first assume intrinsic oscillator losses to be absent (i.e. $Q = \infty$, but $\eta \neq 0$). The energy lost upon impact is obtained via the relation $v' = \sqrt{\eta}\, v$ between the speeds before (v) and after (v') impact: $\left(v^2 - v'^2\right)/2 = v^2\left(1 - \eta\right)/2$. This must equal the energy gained by acceleration in the electric field, $2\mathcal{V}^2$ in our units. Equating the two yields the velocity before impact:

$$v^2 = 4\mathcal{V}^2/\left(1 - \eta\right). \tag{2}$$

Now we can obtain the one-way travel time τ_0. We assume the last impact was at $z(0) = -1$, with $\dot{z}\left(0^+\right) = v'$. Based on the solution $z(\tau) = \mathcal{V}^2 + v' \sin(\tau) - \left(1 + \mathcal{V}^2\right)\cos(\tau)$, we demand $z(\tau_0) = +1$. This yields τ_0 via $\sin\tau_0 = \left[-B + \sqrt{B^2 - 4AC}\right]/2A$, with $A = v'^2 + \left(1 + \mathcal{V}^2\right)^2$, $B = 2v'\left(\mathcal{V}^2 - 1\right)$, and $C = -4\mathcal{V}^2$.

Despite the impact damping, self-oscillations are possible down to the lowest voltages for $Q = \infty$, because the grazing impact of the shuttle minimizes the loss: impact velocity $v \to 0$ for $\mathcal{V} \to 0$. In this limit, the one-way travel time is just half the intrinsic oscillator period ($\tau_0 = \pi$), i.e. the impact happens exactly at the turning point of the oscillatory motion, with the shuttle barely touching the electrode. Consequently, τ_0 then turns out to be independent of the impact damping parameter η. For *small voltages*, we obtain $\pi - \tau \approx 2\mathcal{V}\left(1 + \sqrt{\eta}\right)/\sqrt{1 - \eta}$. This relation represents the decrease of the travel time from its zero-voltage value, to first order in $\mathcal{V}$, and it could serve to extract the impact damping η. At *high voltages* ($\mathcal{V} \gg 1$), one would observe $I \propto \mathcal{V}^2$, as higher accelerations lead to shorter travel times. However, current experimental parameters [30] indicate that typically $\mathcal{V}^2 \lesssim 10^{-2}$, which suggests that the high-voltage regime is not reached.

We now reconsider the intrinsic oscillator damping (thus $Q < \infty$), where a minimum voltage has to be applied for self-oscillations [18, 32] in order to overcome the frictional losses. This voltage can be obtained by demanding the total loss (both by impact damping and mechanical friction) during one half-cycle to equal the energy gain by electrostatic acceleration. This then defines the threshold dc voltage for the shuttle's self-oscillations in the absence of driving:

$$\mathcal{V}_{\text{thr}}^2 = \frac{\pi}{4} Q^{-1}\,. \tag{3}$$

Numerical calculations for the experimentally relevant parameters suggest that apart from the appearance of this threshold voltage there is no appreciable modification of the shuttle dynamics above threshold as long as Q is large [30].

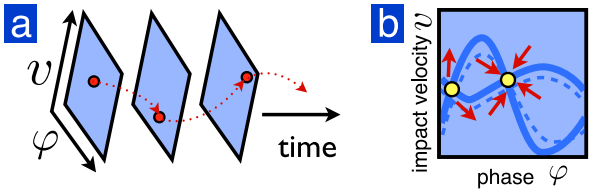

Figure 2. Nonlinear map for the impact dynamics of an electron shuttle. Phase φ of the external drive and impact velocity v are displayed at each impact event. (a) The evolution maps $\left(\varphi_n,\, v_n\right)$ into $\left(\varphi_{n+1},\, v_{n+1}\right)$ upon the next impact at the same electrode. This map completely encodes the dynamics. (b) Fixed-points, both attractive and repulsive, arise in the $(\varphi,\, v)$-plane for suitable parameters. These are intersections of the curves where $v_{n+1} = v_n$ or $\varphi_{n+1} = \varphi_n$ (shown here). Small parameter changes usually do not change the number and type of fixed points, which makes synchronization robust.

2.2. General nonlinear map in the presence of driving

Much more complex nonlinear behavior may arise under sufficiently strong additional oscillatory driving.

For a given impact event at $z = -1$ and time $\tau^{(n)}$, the pair $\left(v_n,\ \varphi_n\right)$ of the initial velocity v_n and the phase $\varphi_n = \Omega\tau^{(n)}$ of the external oscillating force, completely determine the shuttle evolution towards the next impact at $z = -1$ (usually with an intermediate impact at $z = 1$). The new values φ_{n+1} and v_{n+1} follow from the unique mapping (cf figure 2):

$$\varphi_{n+1} = \varphi'\left(\varphi_n,\, v_n\right), \tag{4}$$

$$v_{n+1} = v'\left(\varphi_n,\, v_n\right). \tag{5}$$

Note that in the absence of an external drive, there would be only a one-dimensional relation $v_{n+1} = v'\left(v_n\right)$ with a simple fixed-point $\tilde{v} = v'\left(\tilde{\varphi},\, \tilde{v}\right)$. That is the regular shuttling already discussed above.

3. Synchronization of an impacting shuttle to an external drive

Although it is known that such two-dimensional nonlinear mappings can generate both complex attractors with a period larger than one cycle and chaotic dynamics our analysis focuses on the case of greatest potential impact for applications. This is synchronization to an external drive (injection locking), which allows to operate a nanomechanical shuttle as a rectifier [40]; it may also be exploited to lock the shuttle dynamics to a very precise external frequency source even for a rather weak drive. Thus the nonlinear dynamics can be turned from a complication into a useful tool. In addition, the framework presented here can form the basis for discussing higher-order fixed-points and chaotic motion in shuttles and similar impacting systems in general.

3.1. Numerical simulation of the phase dynamics

At small external driving strength, there is no simple fixed-point. This is because the phase just proceeds according to $\varphi_{n+1} \approx \varphi_n + 2\Omega\tau_0$, with τ_0 the one-way travel time in the absence of

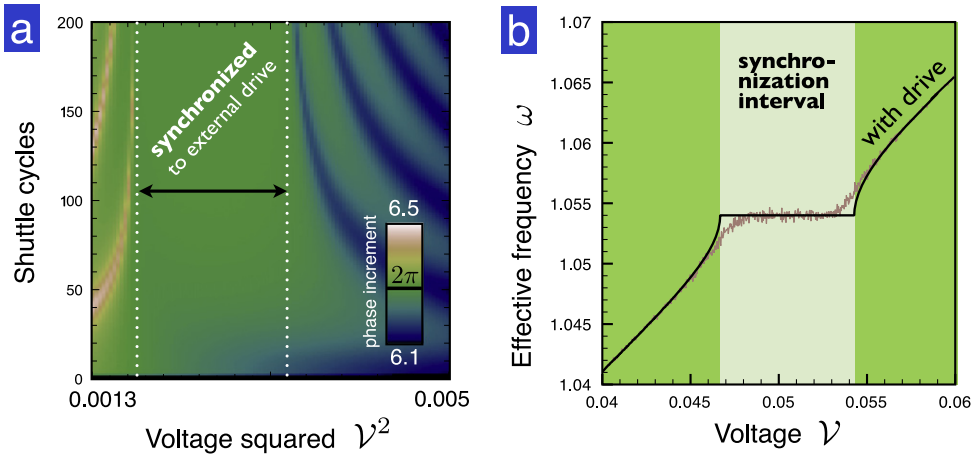

Figure 3. Synchronization of an impacting electron shuttle to an external drive. (a) The phase increment $\varphi_{n+1} - \varphi_n$ of the external drive between two impacting events is shown as a color-code. As time progresses (vertical axis, measured in shuttle cycles), the phase increment either displays a slow beating pattern, or it may lock to a value of 2π, signalling synchronization. This happens inside a certain interval, as the dc shuttle voltage (or any other parameter) is varied, shifting the shuttle's eigenfrequency. ($\eta = 0.2$, $Q = 10^3$, $\mathcal{F} = 10^{-3}$, $\Omega = 1.054$) (b) The effective, time-averaged shuttle frequency $\omega = \pi/\bar{\tau}$ is plotted versus an external parameter (the voltage). Inside the synchronization interval, the shuttle becomes robust against noise (brown curve)—the curve shown here was obtained for fluctuations $\Delta\Omega = 0.02$ in the driving frequency (see main text) and is evaluated after 6000 impact events. The fluctuations decrease for longer averaging times.

driving. Generally, $2\tau_0\Omega$ is not an integer multiple of 2π, and so there is no definite phase relation between the external driving and the shuttling. The combination of the shuttle's impact dynamics and the weak incommensurate driving makes the shuttle motion lose its exact periodicity. As a result, the shuttle's round-trip time $2\tau_0$ effectively changes slightly from step to step. Figure 3(a) depicts the phase increment $\varphi_{n+1} - \varphi_n$ as a function of time and shows long-term beating patterns. However, when changing the shuttle's parameters (e.g. the voltage), the shuttle's intrinsic period shifts until it becomes almost commensurate with the external drive frequency. Then synchronization may set in (figure 3).

3.2. Adler equation for a nanomechanical shuttle

Mathematically, this corresponds to the generation of a stable period-one fixed point $\tilde{\varphi} = \varphi'(\tilde{\varphi}, \tilde{v})$, $\tilde{v} = v'(\tilde{\varphi}, \tilde{v})$. We now examine the appearance of this phenomenon both numerically and analytically. Numerical observations indicate that the system, once started anywhere in the (φ, v)-plane, quickly relaxes to a 1d manifold that can be described by the phase coordinate alone (figure 4(a)). Therefore, we focus on the phase map and expand it as

$$\varphi_{n+1} = \varphi_n + 2\Omega\tau_0 + K \sin\left(\varphi_n - \varphi_*\right) + \ldots . \tag{6}$$

Here the values of K and φ_* depend on the detailed microscopic parameters, with the coupling K growing from zero upon increasing the drive, and the omitted terms are higher harmonics.

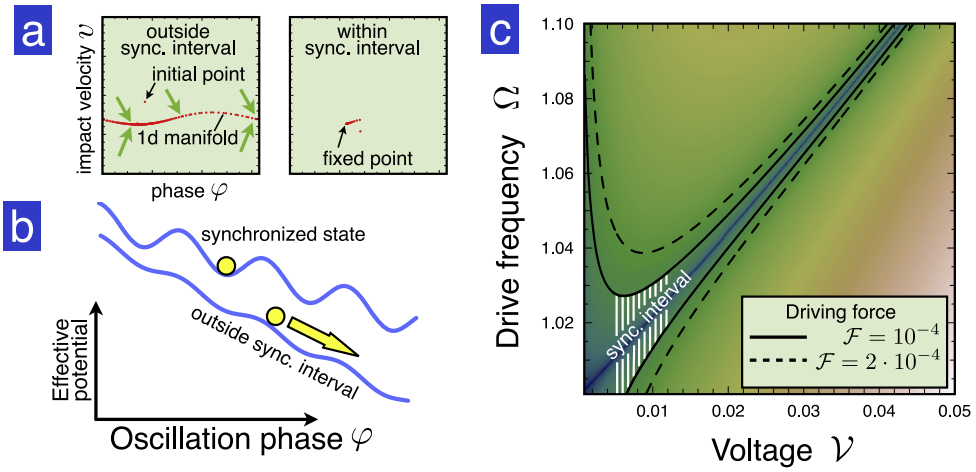

Figure 4. Phase dynamics in an impacting electron shuttle. (a) After only a few impact events, the system dynamics quickly settles onto a 1d manifold, permitting a theory for the phase dynamics alone. (b) The resulting ADLER equation corresponds to a particle sliding in a washboard potential. (c) The predicted synchronization interval (bounded by the contour lines shown here, partially hatched) as a function of drive frequency, plotted using our approximate analytical prediction for the effective ADLER coupling constant of a driven impact shuttle, equation (7). ($\eta = 0.7$.)

Let us denote the deviation of the drive frequency from the undriven shuttling frequency as $\delta\Omega = \Omega - \pi/\tau_0$. If this is small enough, then we obtain a fixed point ($\varphi_{n+1} = \varphi_n = \tilde{\varphi}$), with some phase lag $\tilde{\varphi}$ between shuttling and drive, where $2\tau_0\delta\Omega = K \sin\left(\tilde{\varphi} - \varphi_*\right)$. This requires $\left|2\Omega\tau_0 - 2\pi\right| = \left|2\delta\Omega\tau_0\right| < K$, which defines the synchronization interval, i.e. the permissible deviation $\delta\Omega$. Outside that interval, the phase drifts across the full range $\left[0, 2\pi\right]$, with a varying velocity. Near synchronization, we can assume small phase increments, and the phase map of equation (6) can be written as a differential equation by replacing $\varphi_{n+1} - \varphi_n - 2\pi \approx 2\tau_0 d\varphi/d\tau$, introducing the time-dependent phase shift $\varphi(\tau)$. This yields ageneric equation proposed by ADLER to treat phase-locking phenomena [41, 42]. Integrating the ADLER equation exactly one finds periodic dynamics for the phase increment in each cycle, with a period diverging as $\left|2\tau_0\delta\Omega - K\right|^{-1/2}$ near synchronization. Direct simulations (figure 3) of the nonlinear shuttle dynamics under drive and dc voltage confirm this picture showing, outside the synchronization interval, a periodic modulation with the period diverging near the onset of synchronization.

3.3. Microscopic derivation of the ADLER constant

While ADLER-type equations appear generically in synchronization physics, they become predictive only when we are able to connect the coupling K to the microscopic parameters of the specific model. To this end we repeat the calculation of the one-way travel time for the driven oscillator, obtaining the correction $\delta\tau$ to the travel time τ_0 in the leading order of the driving $\mathcal{F}$. This also involves finding the change in the impact velocity by a new self-consistency equation, where we exploit that the velocity quickly relaxes to the limit cycle while the phase dynamics are much slower. We defer the rather lengthy calculation to the appendix and just state that $\delta\tau$

becomes a harmonic function of φ. The corresponding correction to the phase increment is $\delta\varphi = 2\Omega\delta\tau\,(\varphi)$ and the Adler coupling constant K reads

$$K\left(\mathcal{F}, \Omega\right) = \frac{\Omega\mathcal{F}}{\left(1-\Omega^2\right)v_0}\left|\left(e^{i\Omega\tau_0}-1\right)\left(Z\left(\tau_0, \Omega\right)+S_f\left(\tau_0, \Omega\right)\right)\right|. \tag{7}$$

Here $v_0 = 2\mathcal{V}/\sqrt{1-\eta}$ is the impact velocity without drive (see above). $Z\left(\tau_0, \Omega\right)$ and $S_f\left(\tau_0, \Omega\right)$ are harmonic functions of their arguments, depend on the impact damping parameter η and the velocity v_0, and are defined in the appendix. Equation (7) is given under the simplifying but realistic assumptions of large $Q \gg 1$ and accurately matches the numerical results for sufficiently low drive $\mathcal{F}$.

The synchronization interval $\left|\delta\Omega\right| < K/\left(2\tau_0\right)$ grows linearly with drive strength and increases for lower voltages (while shifting towards lower frequencies; cf figure 4(c)). At very small voltages, modifications occur due to intrinsic damping (finite Q), which destroys the self-oscillations.

3.4. Stability against noise

The existence of an extended synchronization interval implies an increased robustness of the shuttling against noise. Within this interval, the Adler equation describes a phase particle trapped in a local minimum of a washboard potential (figure 4(b)). There the effective shuttle frequency is completely insensitive to a slow drift of system parameters (voltage, effective capacitance, damping, etc). In contrast, time-dependent noise may give rise to phase slips by lifting the particle over the barrier. However, this process is exponentially suppressed when moving towards the middle of the synchronization plateau [43]. We have confirmed this by direct simulations of noise: a noisy impact parameter η does not show any effect on the synchronization range both in a numerical and a leading order perturbative analysis. For a Gaussian distributed noisy driving frequency Ω (which we assume constant between the impact events) we observe phase slips which drive the effective shuttle frequency ω away from $\left\langle\Omega\right\rangle$. They are numerous for voltages at the edges of the former synchronization interval. However, in the center of that interval (e.g. $\mathcal{V} = 0.053$ in figure 3), for a noise value of $\Delta\Omega/\Omega = 0.02$, we observe no phase slips within 300,000 iterations, resulting in a frequency imprecision of at most 10^{-5} in this example. The remaining fluctuations of the effective time-averaged frequency ω decay with time as $1/\sqrt{\tau}$, as expected. Deviations of ω from the drive Ω are exponentially suppressed in the middle of the interval.

While this numerical example illustrates the potential for noise-resistant operation, we note that a full analysis of the frequency fluctuations as well as suitable optimization of parameters is beyond the scope of the present work. The sources of noise, which would have to be characterized carefully in actual experiments, include: thermal mechanical Langevin noise acting on the shuttle (which can be obtained by measuring the shuttle's mechanical quality factor at small oscillations), any fluctuating momentum transfer on impact, possible coupling to other mechanical modes of oscillation due to the nonlinear impact events, charge noise (e.g. 1/f noise from nearby impurities), and mechanical frequency fluctuations and drift (e.g. due to temperature fluctuations) and intrinsic fluctuations of the voltage source.

Applications of single electron devices in metrology demand both a high accuracy in measuring the transmitted charge as well as operation at a sufficiently high current output. For

improving the ('phenomenological') constants describing the three quantum electrical effects represented in the quantum metrology triangle, i.e. the Josephson effect, quantum Hall effect and single electron transport, a minimal frequency imprecision of 10^{-7} is required, and 10^{-8} for testing the consistency of the metrological triangle [22]. In order to serve as a future current standard, a single electron shuttling device must produce a current output clearly beyond 100 pA at a white noise level of 1 fA/$\sqrt{s}$ or less [22]. For example, current single electron transfer experiments reach a level of frequency imprecision of almost 10^{-6} at a current of 150 pA [44].

In our numerical example, the goal for the optimization of device parameters then would be to reduce the effective frequency noise to less than the 10^{-6} [44] that are currently attainable. This should be reachable, e.g., by increasing the external drive strength sufficiently which increases the effective barriers in the washboard potential, preventing phase slips.

4. Possible experimental realization

Figure 1(a) depicts a possible experimental realization that would strongly suppress cotunneling events. Here, doubly-clamped, tensile-stressed silicon nitride string resonators with linear quality factors of several 100,000 [45, 46] can be efficiently and controllably driven to sufficiently high (impacting) amplitudes of several 10 nm using dielectric gradient field actuation [47] (acoustic [25] or capacitive drive [23, 24] can be used in similar contexts). Thus, during tunneling, the island is always tens of nanometers away from at least one electrode. The requirement that the charging energy dominates k_BT can be satisfied with an island-electrode capacitance in the attofarad range, imposing experimentally accessible typical island cross sections of tens of nanometers. With these prerequisites within reach [25, 48], the ideas presented here would enable quantitatively reliable current measurements with a mechanical shuttle.

5. Conclusions

In this paper we have analyzed nanomechanical single electron shuttles in the impact regime. We predict that synchronization to an external driving frequency can occur and can be exploited to achieve a very precise shuttle current. This has immediate applications in the active experimental research on mechanical electron shuttles.

In the future, it might also be interesting to study alternative configurations like two nearby electron shuttles which can be coupled (mechanically or capacitively) and whose oscillations can synchronize. This will lead to nontrivial current correlations.

Acknowledgments

Financial support by the Deutsche Forschungsgemeinschaft via Projects No. Ko 416/18 (DS, EW), FOR 635 (MM), an Emmy-Noether grant, the German Excellence Initiative via the Nanosystems Initiative Munich (NIM) and LMU excellent, as well as the European Commission under the FET-Open project QNEMS (233992) is gratefully acknowledged.

Appendix A. Microscopic derivation of the Adler constant

The Adler equation has been introduced as an effective ansatz for the phase map (6). The phase map relates the total phase increment during one full cycle of an externally driven motion to the sum of two terms:

$$\Delta\varphi = \varphi_{n+1} - \varphi_n = 2\Omega\tau_0 + \mathrm{K}\sin\left(\varphi_n - \varphi_*\right).$$

The first term describes the (trivial) propagation of the phase under the driving frequency. The second term represents a periodic function of the phase itself and accounts for the nonlinearity in the phase evolution. Note that any non trivial periodic function would form a nonlinear term in the phase map. As there is no *a priori* criterion for picking a particular periodic function, a harmonic function is normally chosen as the simplest ansatz. The constant of proportionality, the so-called Adler constant K, is usually treated as an effective (fitting) parameter. In this article, however, we directly calculate the Adler constant from the underlying microscopic dynamics—to our knowledge for the first time.

We approach the phase increment $\Delta\varphi\left(\mathcal{F}\right) = \Omega\Delta\tau\left(\mathcal{F}\right)$ by evaluating the variation of the total travel time $\Delta\tau\left(\mathcal{F}\right)$ of the oscillator caused by the external driving during one full oscillation cycle. This includes the forward and backward trajectory and two impact events (at the left and the right contact). We work to leading order in the driving strength $\mathcal{F}$ which resembles the force of a linear response calculation. It will turn out that a periodic function of the phase variable and, in consequence, Adler's constant K can be simply read off. In the following, we collect various contributions to the leading order variation in $\mathcal{F}$.

A.1. Variation of the trajectory by external driving

We take the solution of the undamped and undriven oscillator $z_0(\tau)$ as the reference trajectory. The variation of the trajectory under driving is $\delta z(\tau)$. With the ansatz $z(\tau) = z_0(\tau) + \delta z(\tau)$ equation (1) reduces to

$$\delta\ddot{z}(\tau) = -\delta z(\tau) + \mathcal{F}\cos\left(\Omega\tau\right). \tag{A.1}$$

We solve this reduced equation of motion using the ansatz

$$\delta z(\tau) = A\cos\left(\tau + \xi\right) + \frac{\mathcal{F}}{1-\Omega^2}\cos\left(\Omega\tau + \Phi\right). \tag{A.2}$$

As there is no change to the impact position we keep the spatial boundary conditions fixed $\delta z\big|_{\tau=0} = 0$ but allow for changes of the velocity $\delta\dot{z}\big|_{\tau=0} = \delta v'(0)$. From these boundary conditions we determine the missing constants A and ξ of the ansatz

$$A\cos\left(\xi\right) = -\frac{\mathcal{F}}{1-\Omega^2}\cos\left(\Phi\right) \tag{A.3}$$

$$-A\sin\left(\xi\right) = \delta v'(0) + \frac{\mathcal{F}}{1-\Omega^2}\Omega\sin\left(\Phi\right). \tag{A.4}$$

Inserting these expressions into the ansatz gives the following solution for the variation of the trajectory. We define $g(\tau)$ for later reference.

$$\delta z\left(\tau;\,\Phi\right) = \mathcal{F}v_0 f\left(\tau,\,\Phi\right) + \delta v'(0)\sin\left(\tau\right) \tag{A.5}$$

$$\delta\dot{z}\left(\tau;\,\Phi\right) = \mathcal{F}v_0 \dot{f}\left(\tau,\,\Phi\right) + \delta v'(0)\cos\left(\tau\right) \tag{A.6}$$

$$f\left(\tau,\,\Phi\right) = \frac{1}{\left(1-\Omega^2\right)v_0}\left[\cos\left(\Omega\tau+\Phi\right) - \cos\left(\Phi\right)\cos\left(\tau\right) + \Omega\sin\left(\Phi\right)\sin\left(\tau\right)\right] \tag{A.7}$$

$$g\left(\tau\right) = \sin\left(\tau\right)/v_0\left(\tau_0\right). \tag{A.8}$$

A.2. Leading order correction to the one-way travel time

Any variation in the trajectory may lead to a variation of the one-way travel time between two impacts $\tau_{\text{impact}} = \tau_0 + \delta\tau$. We determine this variation for the one-way travel time around the undriven travel time τ_0. Note that this variation consists of two parts, one directly related to the variation of the trajectory under drive, the other originating from a change of the velocity of the oscillator. This velocity change will be discussed self-consistently. Yet until that point, effectively two (dependent) variational parameters dv and $\mathcal{F}$ will be considered.

$$\delta\tau = -\frac{\delta z\left(\tau_0\right)}{\dot{z}\left(\tau_0\right)} = -\mathcal{F}f\left(\tau_0,\,\Phi\right) - \delta v'(0)g\left(\tau_0\right) \tag{A.9}$$

Within this approximation, we replace the perturbed velocity by the unperturbed one $\dot{z}\left(\tau_0;\,\Phi\right) = v_0\left(\tau_0\right)$.

A.3. Leading order corrections to the velocity at the second impact

The velocity shortly before the second impact is expanded around the corresponding velocity of the undriven case up to linear order in the variation w.r.t. the one-way travelling time and the velocity

$$\begin{aligned}\dot{z}\left(\tau_0+\delta\tau\right) &= \dot{z}_0\left(\tau_0+\delta\tau\right) + \delta\dot{z}\left(\tau_0+\delta\tau\right)\\ &\overset{\text{l.o.}}{=} \dot{z}_0\left(\tau_0\right) + \ddot{z}_0\left(\tau_0\right)\delta\tau + \delta\dot{z}\left(\tau_0\right).\end{aligned}$$

We insert the expressions for $\delta\tau$ and $\delta\dot{z}\left(\tau_0\right)$ to obtain the velocity at impact

$$\delta v\left(\tau_0+\delta\tau\right) = \mathcal{F}R_f\left(\Phi\right) + \delta v'(0)R_v \tag{A.10}$$

The driving $\mathcal{F}$ and the initial velocity variation $\delta v'(0)$ can be regarded as forces in a linear response approach. For convenience, we denote the response functions

$$R_f\left(\Phi\right) = v_0\dot{f}\left(\tau_0,\,\Phi\right) - \ddot{z}_0\left(\tau_0\right)f\left(\tau_0,\,\Phi\right) \tag{A.11}$$

$$R_v = v_0\left(\tau_0\right)\dot{g}\left(\tau_0\right) - \ddot{z}_0\left(\tau_0\right)g\left(\tau_0\right). \tag{A.12}$$

The one-way travel time $\tilde{\tau}$ and the velocity variation $\delta\tilde{v}$ on the backward path can be obtained analogously with the replacements $\delta v'(0) \to \delta v'\left(\tau_0+\delta\tau\right) = \sqrt{\eta}\,\delta v\left(\tau_0+\delta\tau\right)$ (initial velocity variation), $\Phi \to \tilde{\Phi} = \Phi + \Omega\left(\tau_0+\delta\tau\right)$ (propagated phase), and $\mathcal{F} \to -\mathcal{F}$ (force acting towards the opposite direction).

$$\begin{aligned}
\delta\tilde{\tau} &= \mathcal{F}f\left(\tau_0, \tilde{\Phi}\right) - \delta v\left(\tau_0 + \delta\tau\right)\sqrt{\eta}\, g\left(\tau_0\right) \\
&= \mathcal{F}f\left(\tau_0, \tilde{\Phi}\right) - \mathcal{F}g\left(\tau_0\right)\sqrt{\eta}R_f\left(\Phi\right) - \delta v'(0)g\left(\tau_0\right)\sqrt{\eta}R_v \\
\delta v\left(T\right) &= -\mathcal{F}R_f\left(\tilde{\Phi}\right) + \sqrt{\eta}\,\delta v\left(\tau_0 + \delta\tau\right)R_v \\
&= -\mathcal{F}R_f\left(\tilde{\Phi}\right) + \mathcal{F}\sqrt{\eta}R_f\left(\Phi\right)R_v + \delta v'(0)\sqrt{\eta}R_v^2.
\end{aligned}$$

Steady state velocity. We assume that the velocity relaxes quickly to the steady state value. In the following we only consider cycles with exactly two impact events but no other turning points, i.e. the full period of the motion is $T \approx 2\tau_0$. Then the steady state velocity can be calculated self-consistently from the condition

$$\delta v'\left(T\right) = \delta v'(0).$$

Inserting the above result for $\sqrt{\eta}\,\delta v\left(T\right)$ we solve for $\delta v'$. The steady state velocity is a harmonic function of the phase Φ

$$\delta v' = \mathcal{F}\sqrt{\eta}\frac{-R_f\left(\tilde{\Phi}\right) + \sqrt{\eta}R_f\left(\Phi\right)R_v}{1 - \eta R_v^2}. \tag{A.13}$$

A.4. Total phase shift during one cycle

The total phase shift during one full cycle is

$$\begin{aligned}
\delta\Phi/\Omega &= \delta\tau + \delta\tilde{\tau} \\
&= \mathcal{F}\Big[f\left(\tau_0, \tilde{\Phi}\right) - f\left(\tau_0, \Phi\right) - g\left(\tau_0\right)\sqrt{\eta}R_f\left(\Phi\right)\Big] - \delta v'(0)g\left(\tau_0\right)\left(1 + \sqrt{\eta}R_v\right) \\
&= \mathcal{F}\Big[f\left(\tau_0, \tilde{\Phi}\right) - f\left(\tau_0, \Phi\right)\Big] + \mathcal{F}g\left(\tau_0\right)\sqrt{\eta}\frac{R_f\left(\tilde{\Phi}\right) - R_f\left(\Phi\right)}{1 - \sqrt{\eta}R_v}.
\end{aligned}$$

A.5. Analytic expression for Adler constant

An analytic expression for the Adler constant K is most easily extracted using a complex representation of the phase dependent terms. We write $\cos\left(x\right) = \Re\left[e^{ix}\right]$, $\sin\left(x\right) = \Re\left[-ie^{ix}\right]$ and use the linearity of the real part to express

$$f\left(\tau_0, \Phi, \Omega\right) = \Re\left[e^{i\Phi}\frac{Z\left(\tau_0, \Omega\right)}{\left(1 - \Omega^2\right)v_0}\right] \tag{A.14}$$

$$Z\left(\tau_0, \Omega\right) = e^{i\Omega\tau_0} - \cos\left(\tau_0\right) - i\Omega\sin\left(\tau_0\right) \tag{A.15}$$

$$R_f\left(\Phi, \Omega\right) = \Re\left[e^{i\Phi}\frac{v_0\dot{Z}\left(\tau_0, \Omega\right) - \ddot{z}_0\left(\tau_0\right)Z\left(\tau_0, \Omega\right)}{\left(1 - \Omega^2\right)v_0}\right] \tag{A.16}$$

$$S_f\left(\tau_0, \Omega\right) = \frac{g\left(\tau_0\right)\sqrt{\eta}}{1 - \sqrt{\eta}R_v\left(\tau_0\right)}\left[v_0\dot{Z}\left(\tau_0, \Omega\right) - \ddot{z}_0\left(\tau_0\right)Z\left(\tau_0, \Omega\right)\right].$$

Together with the previously obtained solution for the case without driving

$$\begin{aligned} v_0 &= 2\mathcal{V}/\sqrt{1-\eta} \\ \ddot{z}_0\left(\tau_0\right) &= -v_0\sqrt{\eta}\,\sin\left(\tau_0\right) + \left(1 + \mathcal{V}^2\right)\cos\left(\tau_0\right), \end{aligned}$$

we can write the phase advance during one cycle as a harmonic function of the phase Φ

$$\begin{aligned} \delta\Phi &= \frac{F\Omega}{\left(1-\Omega^2\right)v_0}\Re\left[e^{i\Phi}\left(e^{i\Omega\tau_0} - 1\right)\left(Z\left(\tau_0, \Omega\right) + S_f\left(\tau_0, \Omega\right)\right)\right] \\ &= \frac{F\Omega}{\left(1-\Omega^2\right)v_0}\cos\left(\Phi - \varphi\left(\tau_0, \Omega\right)\right)\left|\left(e^{i\Omega\tau_0} - 1\right)\left(Z\left(\tau_0, \Omega\right) + S_f\left(\tau_0, \Omega\right)\right)\right| \end{aligned} \tag{A.17}$$

$\varphi\left(\tau_0, \Omega\right)$ represents a phase shift caused by the nonlinear response of the system. We read off the Adler constant

$$K\left(\mathcal{F}, \Omega\right) = \frac{\Omega\mathcal{F}}{\left(1-\Omega^2\right)v_0}\left|\left(e^{i\Omega\tau_0} - 1\right)\left(Z\left(\tau_0, \Omega\right) + S_f\left(\tau_0, \Omega\right)\right)\right|. \tag{A.18}$$

A.6. Approximate solution

To obtain an approximate solution we assume that the undriven oscillation frequency does not deviate from the eigenfrequency $\omega = 1$ of the oscillator. This means that we neglect the effect of the voltage on the one-way travel time and set $\tau_0 \approx \pi$. In consequence, $S_f\left(\pi, \Omega\right) = 0$. Expanding $\Omega = 1 + \delta\Omega$ then results in

$$K\left(\mathcal{F}\right) = \pi\mathcal{F}/2v_0.$$

Note that in this approximation K is independent of the external driving frequency Ω. Yet the initial approximation did not completely eliminate its dependence on the voltage as the velocity $v_0\left(\mathcal{V}\right)$ remains a function of the voltage.

Applying the approximate solution we give a rough estimate of the synchronization range based on the following argument: In the steady state, the phase increment must be a multiple of 2π, i.e. $\delta\varphi = 2\pi n = 2\Omega\tau_0 + K\,\sin\left(\varphi - \varphi_*\right)$. With $\left|\sin\left(\varphi\right)\right| < 1$ a constraint on the minimal driving strength follows:

$$\mathcal{F} > 4v_0\left|\Omega - \omega\right| = \mathcal{F}_{min}\left(\delta\Omega\right).$$

If the driving frequency matches the eigenfrequency of the shuttle (or one of its higher harmonics) synchronization trivially holds. For small detunings $\delta\Omega$ driving above the minimal driving strength is capable of synchronizing the oszillator.

If the full Ω-dependence of $K\left(\mathcal{F}, \Omega\right)$ is considered in the general solution, the minimal driving strength shows a nonlinear dependence on the detuning. However, for small detunings, the qualitative picture still holds.

References

[1] Cleland A N 2003 *Foundations of Nanomechanics* (Berlin: Springer)
[2] Menno P, Herre S J and Vander Z 2012 Mechanical systems in the quantum regime *Phys. Rep.* **511** 273–335
[3] Jensen K, Kim K and Zettl A 2008 An atomic-resolution nanomechanical mass sensor *Nat. Nanotechnol.* **3** 533–7
[4] Chaste J, Eichler A, Moser J, Ceballos G, Rurali R and Bachtold A 2012 A nanomechanical mass sensor with yoctogram resolution *Nat. Nanotechnol.* **7** 301
[5] Hanay M S, Kelber S, Naik A K, Chi D, Hentz S, Bullard E C, Colinet E, Duraffourg L and Roukes M L 2012 Single-protein nanomechanical mass spectrometry in real time *Nat. Nanotechnol.* **7** 602–8
[6] Mamin H J and Rugar D 2001 Sub-attonewton force detection at millikelvin temperatures *Appl. Phys. Lett.* **79** 3358–60
[7] Rugar D, Budakian R, Mamin H J and Chui B W 2004 Single spin detection by magnetic resonance force microscopy *Nature* **430** 329–32
[8] Moser J, Güttinger J, Eichler A, Esplandiu M J, Liu D E, Dykman M I and Bachtold A 2013 Ultrasensitive force detection with a nanotube mechanical resonator *Nat. Nanatechnol.* **8** 493
[9] O'Connell A D *et al* 2010 Quantum ground state and single-phonon control of a mechanical resonator *Nature* **464** 697–703
[10] Teufel J D *et al* 2011 Sideband cooling of micromechanical motion to the quantum ground state *Nature* **475** 359
[11] Chan J *et al* 2011 Laser cooling of a nanomechanical oscillator into its quantum ground state *Nature* **478** 89–92
[12] Eichler A, Moser J, Chaste J, Zdrojek M, Wilson-Rae I and Bachtold A 2011 Nonlinear damping in mechanical resonators made from carbon nanotubes and graphene *Nat. Nanotechnol.* **6** 339–42
[13] Bagheri M, Poot M, Li Mo, Pernice W P H and Tang H X 2011 Dynamic manipulation of nanomechanical resonators in the high-amplitude regime *Nat. Nanotechnol.* **6** 726–32
[14] Villanueva L G, Kenig E, Karabalin R B, Matheny M H, Lifshitz R, Cross M C and Roukes M L 2013 Surpassing fundamental limits of oscillators using nonlinear resonators *Phys. Rev. Lett.* **110** 177208
[15] Kenig E, Cross M C, Villanueva L G, Karabalin R B, Matheny M H, Lifshitz R and Roukes M L 2012 Optimal operating points of oscillators using nonlinear resonators *Phys. Rev.* E **86** 056207
[16] Karabalin R B, Lifshitz R, Cross M C, Matheny M H, Masmanidis S C and Roukes M L 2011 Signal amplification by sensitive control of bifurcation topology *Phys. Rev. Lett.* **106** 094102
[17] Kim C, Prada M, Platero G and Blick R H 2013 Realizing broadbands of strong nonlinear coupling in nanoelectromechanical electron shuttles *Phys. Rev. Lett.* **111** 197202
[18] Gorelik L Y, Isacsson A, Voinova M V, Kasemo B, Shekhter R I and Jonson M 1998 Shuttle mechanism for charge transfer in coulomb blockade nanostructures *Phys. Rev. Lett.* **80** 4526–9
[19] Keller M W, Martinis J M, Zimmerman N M and Steinbach A H 1996 Accuracy of electron counting using a 7-junction electron pump *Appl. Phys. Lett.* **69** 1804–6
[20] Pekola J P, Vartiainen J J, Möttönen M, Saira O-P, Meschke M and Averin D V 2008 Hybrid single-electron transistor as a source of quantized electric current *Nat. Phys.* **4** 120–4
[21] Steck B, Gonzalez-Cano A, Feltin N, Devoille L, Piquemal F, Lotkhov S and Zorin A B 2008 Characterization and metrological investigation of an R-pump with driving frequencies up to 100 MHz *Metrologia* **45** 482
[22] Scherer H and Camarota B 2012 Quantum metrology triangle experiments: a status review *Meas. Sci. Technol.* **23** 124010
[23] Erbe A, Weiss C, Zwerger W and Blick R H 2001 Nanomechanical resonator shuttling single electrons at radio frequencies *Phys. Rev. Lett.* **87** 096106
[24] Scheible D V, Weiss C, Kotthaus J P and Blick R H 2004 Periodic field emission from an isolated nanoscale electron island *Phys. Rev. Lett.* **93** 186801

[25] Koenig D R, Weig E M and Kotthaus J P 2008 Ultrasonically driven nanomechanical single-electron shuttle *Nat. Nanotechnol.* **3** 482
[26] Moskalenko A V *et al* 2009 Nanomechanical electron shuttle consisting of a gold nanoparticle embedded within the gap between two gold electrodes *Phys. Rev.* B **79** 241403
[27] Kim H S, Qin H and Blick R H 2010 Self-excitation of single nanomechanical pillars *New J. Phys.* **12** 033008
[28] Azuma Y, Kobayashi N, Chorley S, Prance J, Smith C G, Tanaka D, Kanehara M, Teranishi T and Majima Y 2011 Individual transport of electrons through a chemisorbed au nanodot in coulomb blockade electron shuttles *J. Appl. Phys.* **109** 024303
[29] Kim C, Prada M and Blick R H 2012 Coulomb blockade in a coupled nanomechanical electron shuttle *ACS Nano* **6** 651–5
[30] Koenig D R and Weig E M 2012 Dc voltage-sustained self-oscillation of a nano-mechanical electron shuttle *Appl. Phys. Lett.* **101** 213111
[31] Grabert H and Devoret M H 1992 *Single Charge Tunneling* (New York: Plenum)
[32] Shekhter R I, Gorelik L Y, Jonson M, Galperin Y M and Vinokur V M 2006 Shuttle transport in nanostructures *Handbook of Theoretical and Computational Nanotechnology* vol 5 (Valencia, CA: American Scientific Publishers) pp 1–59
[33] Franklin B 1962 Chapter letter from Benjamin Franklin to Peter Collinson dated September 1753 vol 5 *The Papers of Benjamin Franklin* (New Haven, CT: Yale University Press) p 68
[34] Bagheri M, Poot M, Fan L, Marquardt F and Tang H X 2013 Photonic cavity synchronization of nanomechanical oscillators *Phys. Rev. Lett.* **111** 213902
[35] Zhang M, Wiederhecker G S, Manipatruni S, Barnard A, McEuen P and Lipson M 2012 Synchronization of micromechanical oscillators using light *Phys. Rev. Lett.* **109** 233906
[36] Matheny M H, Grau M, Villanueva L G, Karabalin R B, Cross M C and Roukes M L 2013 Synchronization of two anharmonic nanomechanical oscillators *Phys. Rev. Lett.* **112** 014101
[37] Manzano G, Galve F, Giorgi G L, Hernandez-Garcia E and Zambrini R 2013 Synchronization, quantum correlations and entanglement in oscillator networks *Sci. Rep.* **3** 1439
[38] Agrawal D K, Woodhouse J and Seshia A A 2013 Observation of locked phase dynamics and enhanced frequency stability in synchronized micromechanical oscillators *Phys. Rev. Lett.* **111** 084101
[39] Scheible D V and Blick R H 2010 A mode-locked nanomechanical electron shuttle for phase-coherent frequency conversion *New J. Phys.* **12** 023019
[40] Pistolesi F and Fazio R 2005 Charge shuttle as a nanomechanical rectifier *Phys. Rev. Lett.* **94** 036806
[41] Adler R 1946 A study of locking phenomena in oscillators *Proc. IRE* **34** 351
[42] Razavi B 2004 A study of injection locking and pulling in oscillators *IEEE J. Solid-State Circuits* **39** 1415
[43] Pikovsky A, Rosenblum M and Kurths J 2003 *Synchronization: A Universal Concept in Nonlinear Sciences, Cambridge Nonlinear Science Series* (Cambridge: Cambridge University Press)
[44] Giblin S P, Kataoka M, Fletcher J D, See P, Janssen T J B M, Griffiths J P, Jones G A C, Farrer I and Ritchie D A Towards a quantum representation of the ampere using single electron pumps *Nat. Commun.* **3** 930
[45] Verbridge S S, Parpia J M, Reichenbach R B, Bellan L M and Craighead H G 2006 High quality factor resonance at room temperature with nanostrings under high tensile stress *J. Appl. Phys.* **99** 124304
[46] Unterreithmeier Q P, Faust T and Kotthaus J P 2010 Damping of nanomechanical resonators *Phys. Rev. Lett.* **105** 027205
[47] Unterreithmeier Q P, Weig E M and Kotthaus J P 2009 Universal transduction scheme for nanomechanical systems based on dielectric forces *Nature* **458** 1001–4
[48] Weiss C and Zwerger W 1999 Accuracy of a mechanical single-electron shuttle *Europhys. Lett.* **47** 97–103